Optical Engineering

OpticalEngineering.SPIEDigitalLibrary.org

# Axicon aberration leading to short-range nondiverging optical array and elliptical dark hollow beam

Rajeev Dwivedi
Parag Sharma
Virendra Kumar Jaiswal
Ranjana Mehrotra

SPIE.

Rajeev Dwivedi, Parag Sharma, Virendra Kumar Jaiswal, Ranjana Mehrotra, "Axicon aberration leading to short-range nondiverging optical array and elliptical dark hollow beam," *Opt. Eng.* **57**(5), 055106 (2018), doi: 10.1117/1.OE.57.5.055106.

# Axicon aberration leading to short-range nondiverging optical array and elliptical dark hollow beam

**Rajeev Dwivedi,[a,b] Parag Sharma,[a,b,*] Virendra Kumar Jaiswal,[a,b] and Ranjana Mehrotra[b]**
[a]Academy of Scientific and Innovative Research (AcSIR), New Delhi, India
[b]CSIR-National Physical Laboratory, New Delhi, India

**Abstract.** We propose a unique method for producing nondiverging optical array and elliptical hollow beam in a controlled manner using aberration patterns generated from oblique illumination of axicon. The optical arrays with propagation invariance property are persisted for short ranges in the focal depth, whereas diverging array with a constant number of bright spots is produced beyond bottle beam. The measured variation in the geometrical parameters of obliquely illuminated axicon setup has facilitated precise control on the dimension of optical array and shape of the elliptical hollow beam, respectively. The theoretical analysis confirms the experimental results for the generation of short-range nondiverging optical array and elliptical dark hollow beam with fine control. To the best of our knowledge, this is the first experimental approach to extend the potential of axicon beyond generation of Bessel and circular hollow beams.  [DOI: 10.1117/1.OE.57.5.055106]

Keywords: nondiffracting beams; lens aberration; optical array; dark hollow beam.

Paper 180030 received Jan. 5, 2018; accepted for publication Apr. 10, 2018; published online May 17, 2018.

## 1 Introduction

The nondiffracting light fields have shown an increasing number of applications especially in the field of imaging,[1–4] optical tweezing,[5,6] ultrashort laser welding of materials,[7] metrology,[8] medical diagnosis, and surgery.[9,10] One of the special kinds of nondiffracting beam, Bessel beam, has attracted a lot of interest in the past few years due to its propagation-invariant central spot width.[11–15] The Bessel beam is generated by various techniques including axicon-lens assembly,[16] annular slit followed by lens,[17] computer-generated hologram,[18] spatial light modulator,[19] and so on. An axicon is a conical lens, which is commonly used to generate Bessel beam up to a distance of $Z_{max}$ (extended depth of focus) followed by a dark hollow beam (DHB) that propagates continuously in a circular symmetry. However, many applications require the combination of axicon with converging lens to form DHB and dark bottle beam (DBB) in a controlled manner. In the case of DHB, lens is placed at a distance ($Z_0$) smaller than its focal length ($f$) from axicon, whereas in the case of DBB it is placed between $f$ and $Z_{max}$. Unlike DHB, DBB sustains for short range (depending upon $Z_{max}$, $f$, and $Z_0$) after the focal depth of axicon and forms a hollow bottle cavity with a maximum ring radius at lens focus.[16] The ring-shaped DHB and DBB generated after the focal depth of axicon/axicon-lens assembly have extensively used in atom guiding[20,21] and trapping,[22,23] as the repulsive action of the optical dipole force traps particle in its central dark region. The high-intensity-focused ring-shaped DHB (generated from axicon doublets) has been applied in corneal cutting in eye surgery[24] and metal cutting[25] in industries. Also, elliptical dark hollow beam (EDHB) generated from astigmatic lenses (i.e., nonideal conditions) are found to be less affected by atmospheric turbulence and can be used in free-space optical communication.[26] Axicon plays a key role in developing common-path interferometric wavefront sensing techniques.[27]

An axicon has better focusing ability with no requirement of lens adjusting. Lens aberration is one of the bottlenecks for achieving high-resolution laser imaging. However, the aberration region induced at the center of the beam consists a well-defined pattern of two-dimensional (2-D) optical array with varying dimensions on changing geometrical parameters.[28,29] The optical arrays have shown their potential in free-space optical communication,[30–32] optical computing,[33,34] and array of optical tweezers.[35–37] Over the past few decades, different kinds of optical array generators have been proposed, mostly based on gratings,[38–40] interferometers,[41] multimode optical fibers,[32] microaxicon array,[42] and zone plates.[43] The quest for developing methods to improve optical data processing, high-quality imaging, and metrological applications has directed research toward generating optical arrays with significant features. Here, we suggest a unique technique for generating a short-range nondiverging optical array (SRNOA) with desired dimensions/number of spots using oblique illumination phenomenon of axicon. A detailed experimental study of the appearance of aberration spots at the center of the beam intensity profile and its behavior with different geometrical conditions has been performed. Theoretical simulations are also executed to explain the generation of SRNOA, which are found to be in good agreement with the experimental results. Further, we implement geometrical approach to analyze the effect of oblique illumination on the generation of hollow beams from axicon/axicon lens assembly and predict the generation of

*Address all correspondence to: Parag Sharma, E-mail: sharmap2@nplindia.org

0091-3286/2018/$25.00 © 2018 SPIE

EDHB in a controlled manner. In addition, the ring parameters of focused elliptical hollow beam generated from obliquely illuminated axicon-lens doublet are compared with circular hollow beam using diffraction theory. In Ref. 16, study of geometrical structure and paraxial ray tracing of an on-axis illuminated axicon was performed to realize the generation of hollow beams (DHB and DBB), which in practice is quite difficult to obtain; therefore, an investigation into aberration causes due to off-axis illumination condition, in general, is important and desired before using axicon in applications with higher precision. Hence, this study not only finds its significance in generating nondiverging optical array in a controlled manner but also in correcting lens aberrations in axicon-derived optical devices.

## 2 Experimental Setup

A monochromatic light beam, generated from intensity stabilized He–Ne laser (Melles Griot 1 mW, 633 nm), was passes through beam expander (or folded using mirrors and made to travel a long path) to achieve a broader beam area at the entrance plane of the axicon "$A_x$" (diameter 25.4 mm, refractive index 1.515, and apex angle 178 deg). Finally, the Bessel beam followed by a monochromatic DHB or DBB was created. The broadened beam spot was created to reduce the effort for adjusting axicon laterally with a slight change in $\Theta$ (the angle between the optic axis of axicon and propagation direction of incident beam), which can be varied by placing axicon on a rotating stage of least count 0.0055 deg. To control the light intensity at CCD detector, variable neutral density filter (VNDF) was used. Finally, the beam was focused using a converging lens "$L1$" (focal length $f = 120$ mm) placed at a distance $Z_0$ from $A_X$, fulfilling the condition $Z_0 < f$ for DHB, and $f < Z_0 < Z_{\max}$ of axicon for DBB. Lens $L1$ is placed only in the case of axicon-lens assembly and removed in the case of axicon only. The output pattern was recorded using a CCD camera (Q-Imaging 5 MP with pixel size of 3.4 $\mu$m $\times$ 3.4 $\mu$m).

## 3 Results and Discussion

We performed an in-depth study of obliquely illuminated axicon in two parts: (i) investigation into the appearance of optical array in different geometrical conditions and (ii) analysis of the generation of the controlled EDHB after the focal depth of tilted axicon-lens doublet.

### 3.1 *Aberration Spots*

An aberration spot in transverse intensity profile of the beam appears due to the oblique illumination (i.e., making an angle of $\Theta$ with optic axis) of light field on axicon. To observe the effect of geometrical conditions on the intensity profile of the beam generated from oblique axicon, the lens $L1$ was removed from the setup (discussed in Sec. 2). In Fig. 1(A), the number of central spots is increasing symmetrically with an increase in the angle $\Theta$ (as reported in Ref. 44). However, similar variations are also observed with increasing propagation distance $Z$, keeping other geometrical parameters fixed (see Fig. 1).

The images recorded at $Z = 150$ mm with $\Theta = 8$ deg in Figs. 1(A-c) and 1(B-a) slightly differ due to the difference in exposure time of the CCD for the two cases. It is obvious, for perfectly aligned axicon, i.e., $\Theta = 0$ deg, that the pattern-containing aberration spots disappear and do not emerge for any propagation distance $Z$. A converged beam (i.e., with lens $L1$ in the setup) also shows similar variation in bright aberration spots with increasing $\Theta$ and $Z$, respectively, in the focal depth of axicon-lens assembly.

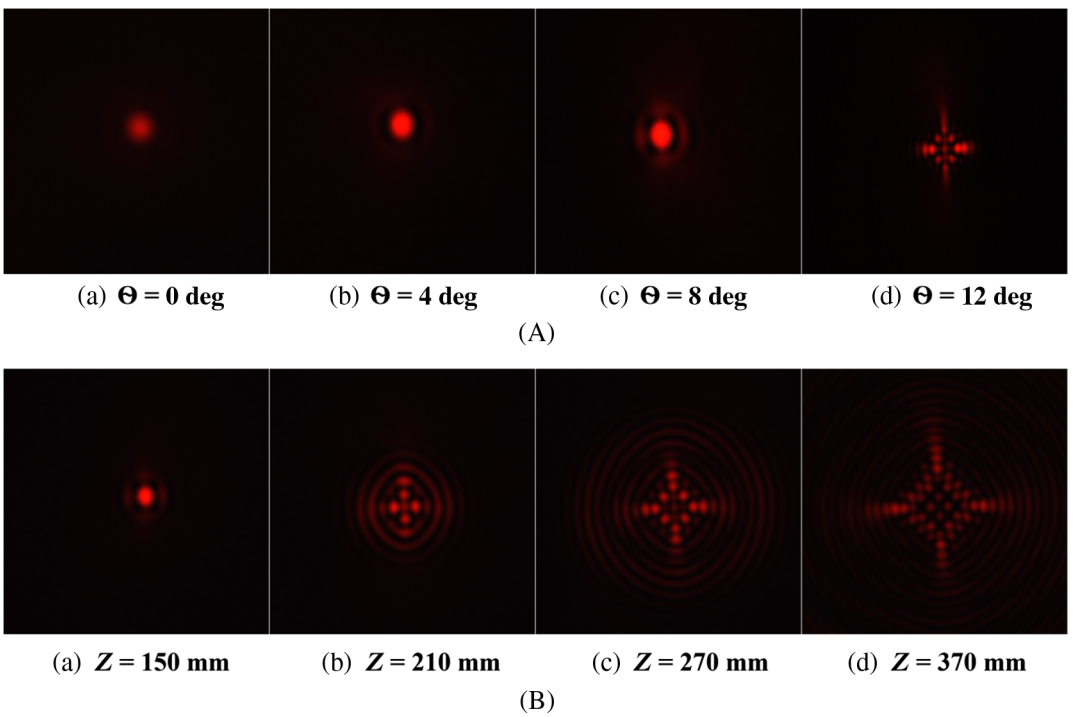


**Fig. 1** CCD images of the aberration spots, (A) with increasing $\Theta$, keeping $Z = 150$ mm, (B) with increasing propagation distance, keeping $\Theta = 8$ deg fixed. In this case, the converging lens $L1$ was removed from the setup.

The number of focal spots, appeared in a well-defined pattern of optical array, is showing increasing dominance over the beam profile with an increase in the angle of tilt of axicon after $\Theta = 4$ deg. Beyond $\Theta = 10$ deg, the array formation in the center of the beam vertically crosses the only visible elliptically shaped band of fringes. However, for a large value of $\Theta$ the intensity of the bright focal spots in the central region of the array decreases as a large number of spots shares the central beam intensity [Figs. 2(g)–2(h)]; hence, large $\Theta$ would be avoided for producing optical array with uniform intensity-focused spots.

Further, the impact of variation in the focal length of $L1$ on the central pattern was studied with two different converging lenses of focal length $f = 120$ mm and $f = 50$ mm. It was found that the change in focal length of a converging lens ($L1$) in the axicon-lens assembly did not show any considerable effect on the formation of the aberration spots; however, it affects the offered $Z_{max}$ of the axicon-lens assembly, which depends upon the focusing power of the converging lens. In the case of DBB (i.e., for $f < Z_0 < Z_{max}$), the regeneration of aberration spots following the bottle cavity region in the propagation distance was observed. As shown in Fig. 3, the regeneration of the aforementioned bright spots array-like structure appeared at $Z_0 = 270$ mm, which becomes clearly visible for $Z_0 > 300$ mm. It was interesting to observe that the number of bright spots in a reappeared pattern remains constant throughout the propagation; however, it was only found to vary with $Z_0$ (keeping other geometrical parameters, such as $\Theta$ and $f$ fixed). This reappearance of aberration spots may be due to the reconstruction property of the Bessel beam; but in this case, the number of bright spots does not increase with the propagation of the beam.

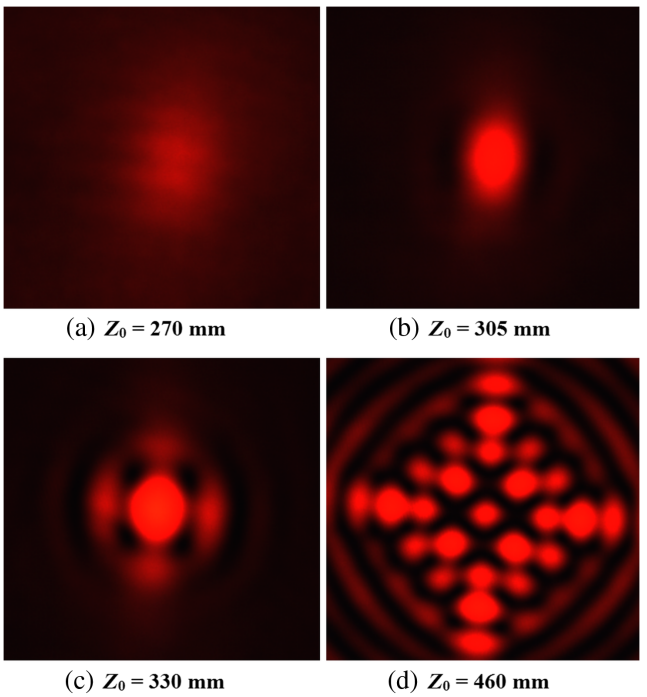


**Fig. 3** (a)–(d) Images of bright spots reappearance in the case of bottle beam for different $Z_0$, keeping $\Theta = 8$ deg and $Z = 1100$ mm fixed.

### 3.1.1 *Nondiverging optical array*

The generation of optical array in the center of the aberration region is an interesting observation as the optical array remains nondiverging for a distance of $dZ \approx 32$ mm from its generation (keeping $\Theta$ fixed), Fig. 4(A). Whereas moving further in the beam propagation direction, the optical array distorted completely and a new array of higher dimension emerges. This emergence and distortion of optical arrays continued till $Z_{max}$. The similar behavior was also observed with changing $\Theta$ (keeping $Z$ fixed) as shown in Fig. 2. The width of the aberration spots was calculated and plotted in Table 1 and shown in Fig. 4(B), respectively, which demonstrates that the width of the aberration spots

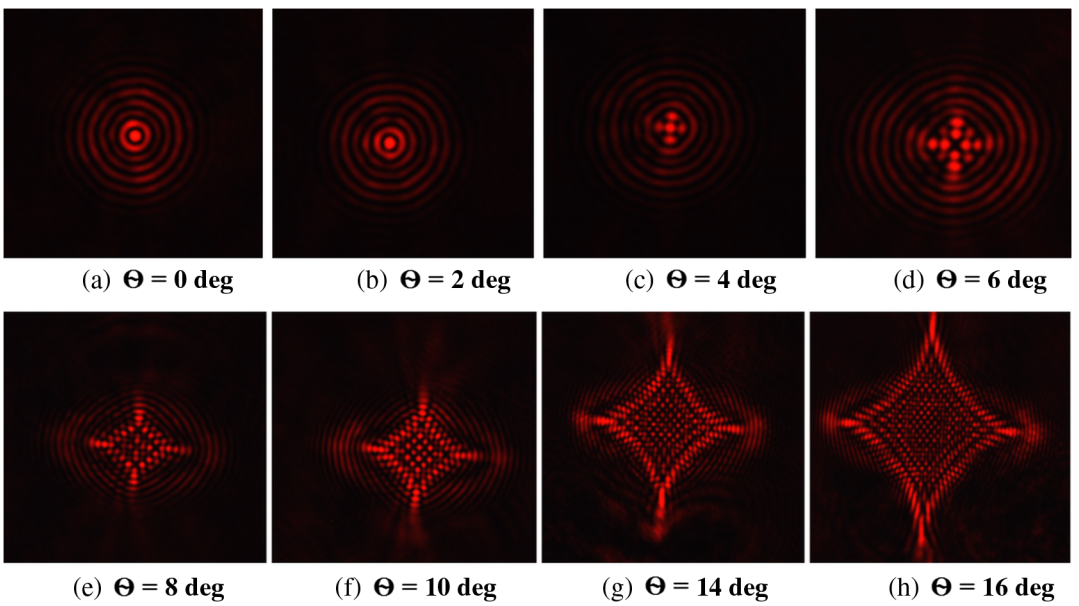


**Fig. 2** (a)–(h) Increase in the number of aberration spots in array with change in $\Theta$, keeping $Z = 85$ mm and $Z_0 = 420$ mm fixed. The converging lens was used with a focal length of $f = 50$ mm.

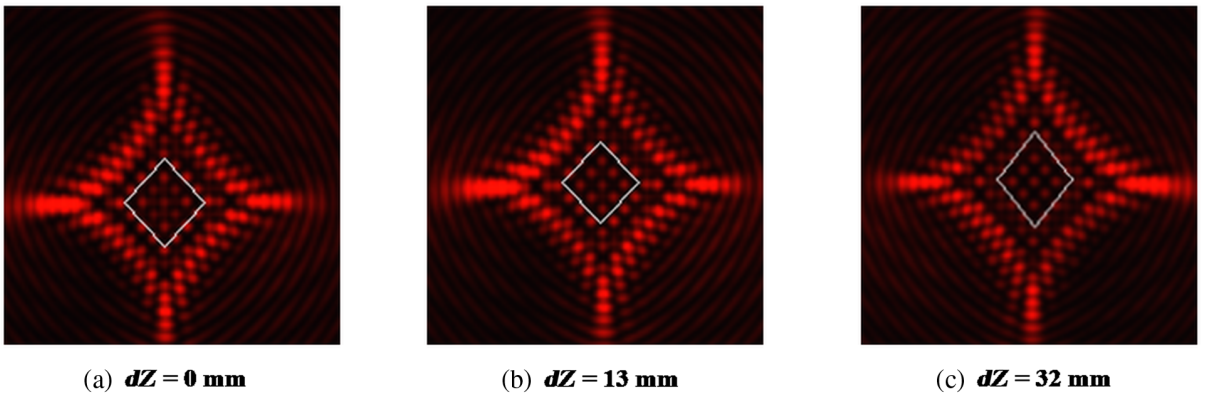

(a) $dZ = 0$ mm (b) $dZ = 13$ mm (c) $dZ = 32$ mm

(A)

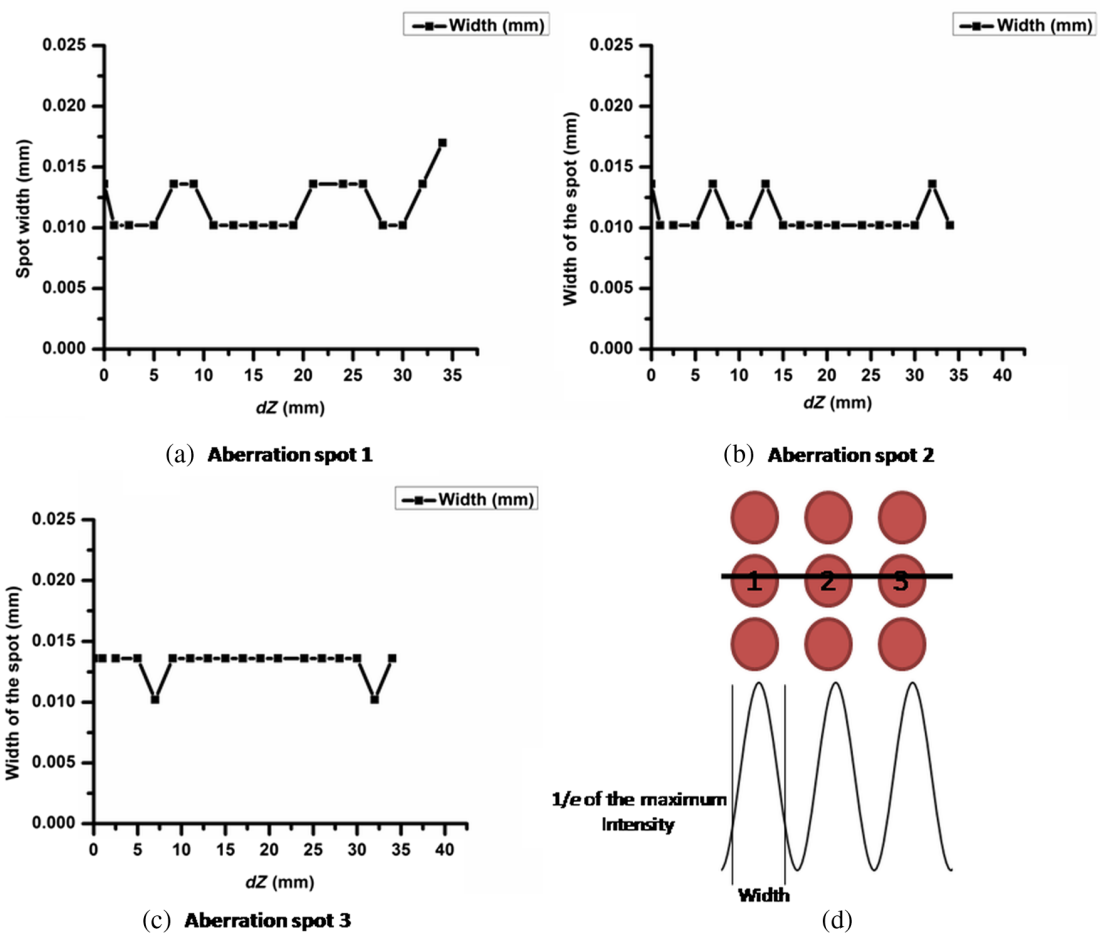


(a) Aberration spot 1 (b) Aberration spot 2

(c) Aberration spot 3 (d)

(B)

**Fig. 4** (A) Generation of a $3 \times 3$ nondiverging optical array in the center of the beam at different propagation distances (keeping $\Theta = 13$ deg fixed) and (B) (a)–(c) variation in the width of the aberration spots with $dZ$. Where $dZ = Z - Z_1$, $Z_1 = 434$ mm is considered as the initial point and $Z$ is the propagation distance. (d) The schematic diagram of method used for calculating width of the aberration spots.

remains invariant with the propagation distance $Z$ for a short range. The measured widths of the aberration spots in the pattern show small variations in the range of 10.2 to 13.6 $\mu$m for a propagation distance of $dZ \approx 32$ mm. This random variation with propagation distance may be due to limitations in manual alignment and image recording. However, the sizes of spots do not vary in a diverging or converging manner in this propagation range, hence can be considered as nondiverging. This nondiverging behavior may be adopted from the parental beam, i.e., central nondiverging spot of the Bessel beam. In Figs. 1 and 2, the dimension of the SRNOA increases with both $Z$ and $\Theta$, respectively, and hence can be controlled by the combination of two.

**Table 1** Calculated values of the width of bright aberration spots in the second row of the $3 \times 3$ optical array for different propagation distances (keeping $\Theta = 13$ deg fixed).

| S. No. | $dZ$ (mm) | Width spot 1 (mm) | Width spot 2 (mm) | Width spot 3 (mm) |
|---|---|---|---|---|
| 1 | 1 | 0.0102 | 0.0136 | 0.0102 |
| 2 | 11 | 0.0102 | 0.0136 | 0.0102 |
| 3 | 21 | 0.0136 | 0.0136 | 0.0102 |
| 4 | 28 | 0.0102 | 0.0136 | 0.0102 |
| 5 | 32 | 0.0136 | 0.0102 | 0.0136 |
| Average width | — | 0.0119 | 0.0110 | 0.0132 |

#### 3.1.2 *Simulations of short-range nondiverging optical array*

The intensity distribution of the optical array can be determined as

$$I(x', y', z) = |E(x', y', z)|^2. \tag{1}$$

In Eq. (1), $E(x', y', z)$ is the field distribution in the observation plane, which can be expressed in terms of Fresnel diffraction integral[45]

$$E(x', y', z) = \frac{1}{i\lambda} \iint E(x, y, 0) \frac{\exp\{ikR\}}{R} \mathrm{d}x' \, \mathrm{d}y', \tag{2}$$

where $R = [(x' - x)^2 + (y' - y)^2 + z^2]^{1/2}$, $k = 2\pi/\lambda$, $\lambda$ is the wavelength, and $E_0(x, y, 0)$ is the light filed distribution in the incident plane of axicon, respectively. As oblique illuminated field forms an elliptical geometry on the incident plane of axicon, an equation of elliptical axicon phase[46] is used to simulate a tilted axicon along with correction parameters $A$ and $B$, respectively. Hence, the phase function of an oblique axicon is defined as

$$\varphi(x, y) = A(n - 1)\alpha(Bx^2 \operatorname{Cos}^2 \Theta + y^2)^{\frac{1}{2}}. \tag{3}$$

The correction parameters can be obtained from analyzing the geometry of the elliptical and circular axicons. The value of the correction parameter $A$ is constant, whereas $B$ ($\geq 1$) varies with $\Theta$ and will be minimum at $\Theta = 0$ deg (i.e., $B = 1$), where it reduces Eq. (3) into phase of an on-axis illuminated ideal-axicon. The field distribution at the exit plane of axicon can be written as

$$E(x', y', z) = \begin{cases} E_0(x, y, 0) \exp[-ik\varphi(x, y)], & r_a < \text{aperture} \\ 0, & r_a \geq \text{aperture} \end{cases}, \tag{4}$$

where $r_a$ is the beam waist. Fresnel diffraction integral in Eq. (1) can be solved using different diffraction methods such as asymptotic integral solving method and Fourier optics.[45] In the present study, we perform Fourier analysis to investigate the generation and propagation dynamics of SRNOA in the focal region of oblique axicon. SRNOA of different dimensions is observed and confirmed the short-range nondiverging behavior (see Figs. 5 and 6).

A small deviation in the propagation distance $Z_1$ in Figs. 4 and 5, might have occurred due to manual measurements errors and thin lens approximation used in simulations. Also, it is evident from Fig. 6 that the short-range nondiverging properties are also persist in $1 \times 1$ and $2 \times 2$ SRNOAs as well, respectively.

It is interesting to observe that the propagation-invariant behavior of these SRNOAs is showing similarity with well-known pattern of the optical modes, generated from complex setups.[32,47–49] Hence, these findings may be useful in developing more simpler and convenient methods for generating the controlled number of modes in the short range of propagation distance. As Bessel beam has the ability to trap atoms in its bright spots,[50] hence the highly focused spots in nondiverging optical array may find its significance in constructing arrays of optical tweezers.

### 3.2 *Elliptical Dark Hollow Beam*

In this section, we perform experimental and geometrical analyses of the effect of oblique illuminated axicon and axicon lens-assembly on the generation of EDHB after the focal depth. Further, numerical study using diffraction theory is performed to examine the variations in the ring parameters of EDHB produced in the focal plane of axicon-lens doublet with $\theta$. As evident from Fig. 2, the oblique illumination of the axicon results in the elliptical bright rings surrounding the central aberration region in the transverse intensity profile of the beam. It is well understood that the elliptical bright

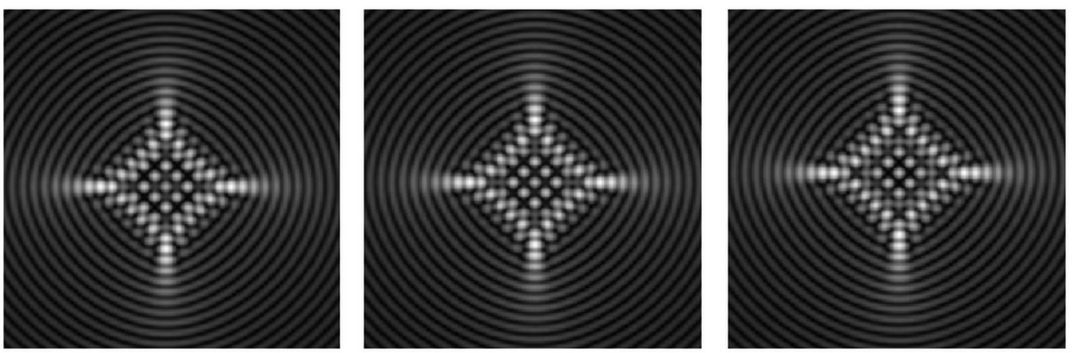

(a) ***dZ* = 0 mm** (b) ***dZ* = 13 mm** (c) ***dZ* = 32 mm**

**Fig. 5** (a)–(c) Numerical simulations of $3 \times 3$ SRNOA at different propagation distances with $n = 1.515$, $\alpha = 0.0174$, $Z_1 = 502$ mm, and $\Theta = 13$ deg fixed.

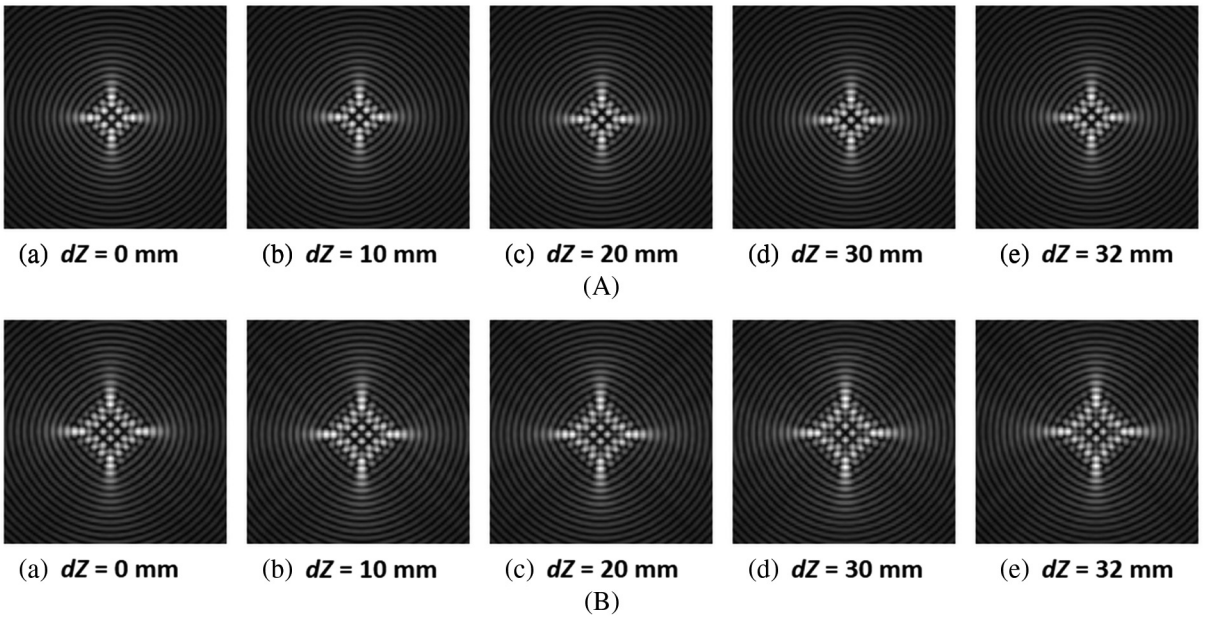


**Fig. 6** Simulated intensity profiles of (A) $1 \times 1$ and (B) $2 \times 2$ SRNOA at $Z_1 = 450$ mm and $Z_1 = 650$ mm, respectively. For both cases $\Theta = 10$ deg, $n = 1.515$, and $\alpha = 0.0174$ remain fixed.

rings in the focal depth of oblique axicon lead to the generation of the EDHB.[26,51] Both theoretical and experimental analyses were performed to understand the effect of different experimental parameters on the shape of the EDHB.

### 3.2.1 *Experimental results*

To investigate the generation of EDHB, an experimental setup was prepared with quantitative control over the angle of oblique illumination of axicon (setup discussed in Sec. 2 was used without lens $L1$).

The angle $\Theta = 8$ deg was kept constant while studying the effect of propagation distance on the transverse intensity profile of beam. Initially, we observed that the central aberration spot pattern surrounded by elliptical rings appears in the depth of focus ($Z_{max}$), beyond which the aberration pattern starts distorting. After propagating a distance of $Z = 5540$ mm from tilted axicon, the center of the beam starts converting into a dark region and leads to the evolution of the EDHB, which continue to expand with propagation as shown in Fig. 7. The experimental analysis shows that the tilt in the position of axicon results in the formation of the DHB,

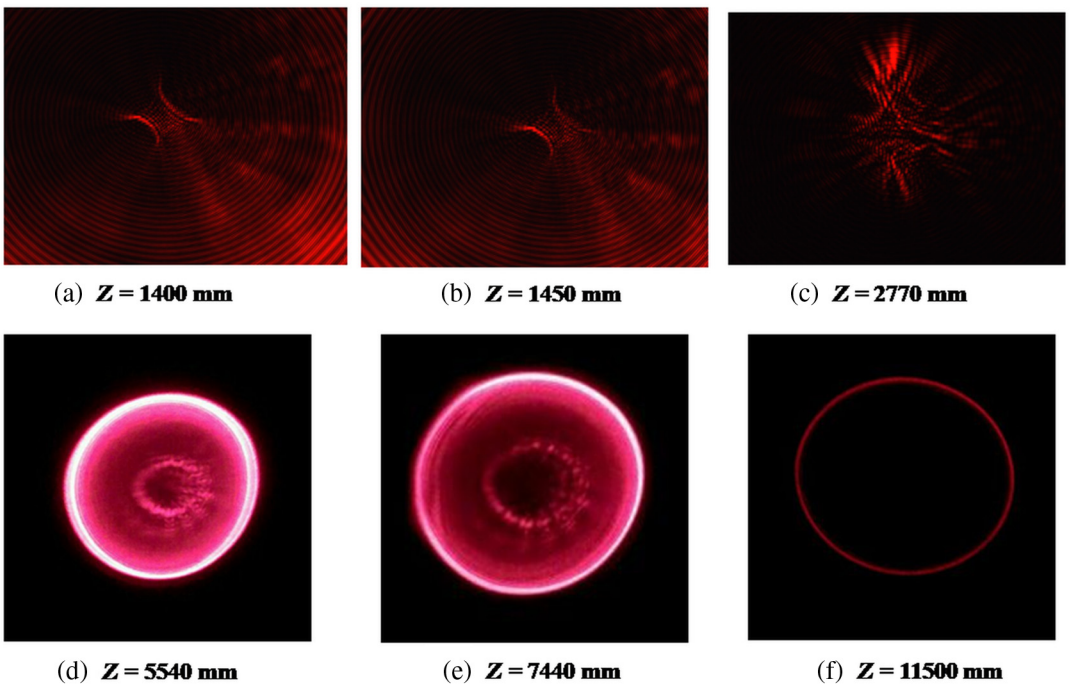


**Fig. 7** (a)–(f) CCD images of the central array structure of the beam developing into a dark region with propagation distance keeping $\Theta = 8$ deg fixed.

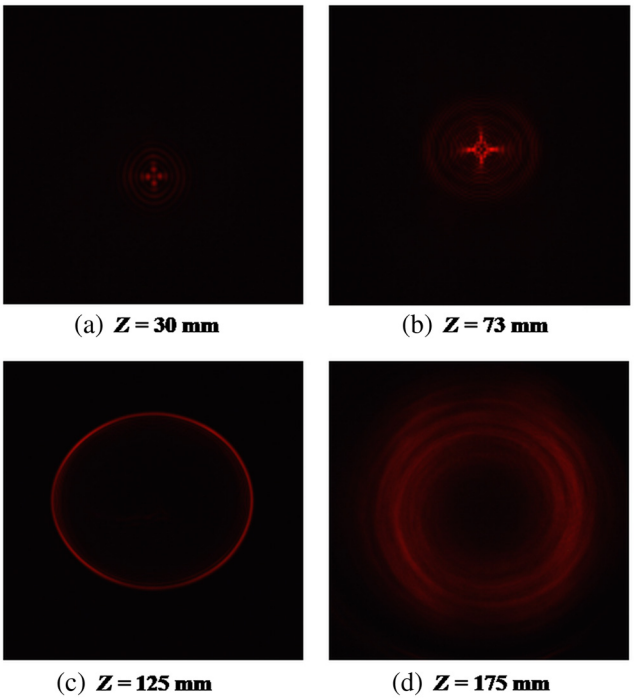


**Fig. 8** The CCD images of the EDHB generated for $Z_0 < f$ at different values of $Z$, keeping the angle of tilt 8 deg fixed.

which is found to be in agreement with the theoretical prediction for a thin axicon [see Eq. (10)].

To analyze the ellipticity of the converged EDHB, a converging lens $L1$ of focal length $f = 120$ mm was used in the setup (expressed in Sec. 2). Now, Fig. 8 shows the generation of EDHB in the case of axicon lens assembly.

### 3.2.2 *Theoretical analysis*

The theoretical simulations were performed to analyze the experimental observations, whereas the variation in the shape of the dark cavity, offered by the DHB with different geometrical constraints is derived below using ray optics.

Perfectly aligned axicon. Figure 9(a) shows that the focal depth $Z_{\max}$ of thin axicon is given as

$$Z_{\max} = \frac{r_a}{\mathrm{Tan}\,\delta_1}, \tag{5}$$

where $\delta_1$ is the angle of deviation introduced by axicon in the propagation direction of the incident beam and defined as $\delta_1 = (n-1)\alpha$. Here, "$n$" is the refractive index and $\alpha$ is the alpha angle of the axicon. In Eq. (6), $r_a = (x^2 + y^2)^{1/2}$ is the radius of the beam illuminated at incident plane of axicon and $(x, y)$ are the co-ordinates of the axicon plane. The conditions, for $x = 0$, $y = r_a$ and for $y = 0$, $x = r_a$, give the intersections of axicon in $x$- and $y$-axes, respectively.

From the ray geometry, the radius of DHB generated after $Z_{\max}$ in $x$- and $y$-axes can be determined as

$$a = (Z\,\mathrm{Tan}\,\delta_1 - r_a). \tag{6}$$

*Tilted axicon*. The axicon is considered as tilted with an angle of $\Theta$ (making with $x$-axis) while keeping propagation direction of the illuminated light field unchanged. As shown in Fig. 9(b), the projection of axicon on $x$-axis and $y$-axis are calculated as $x_1 = r_a\,\mathrm{Cos}\,\Theta$ and $y_1 = r_a$. Therefore, the radius of DHB will not be the same in $x$- and $y$-directions.

$$a_x = (Z\,\mathrm{Tan}\,\delta_1 - r_a\,\mathrm{Cos}\,\Theta), \tag{7}$$

$$a_y = (Z\,\mathrm{Tan}\,\delta_1 - r_a). \tag{8}$$

Therefore, the quantitative variation in the elliptical behavior of the dark region of DHB can be defined in terms of eccentricity

$$e = \left[1 - \left(\frac{a_x}{a_y}\right)^2\right]^{1/2}. \tag{9}$$

*Tilted axicon in axicon-lens assembly*. The light deflected from axicon is again deviated by a thin converging lens; therefore, the total deviation introduced by axicon-lens

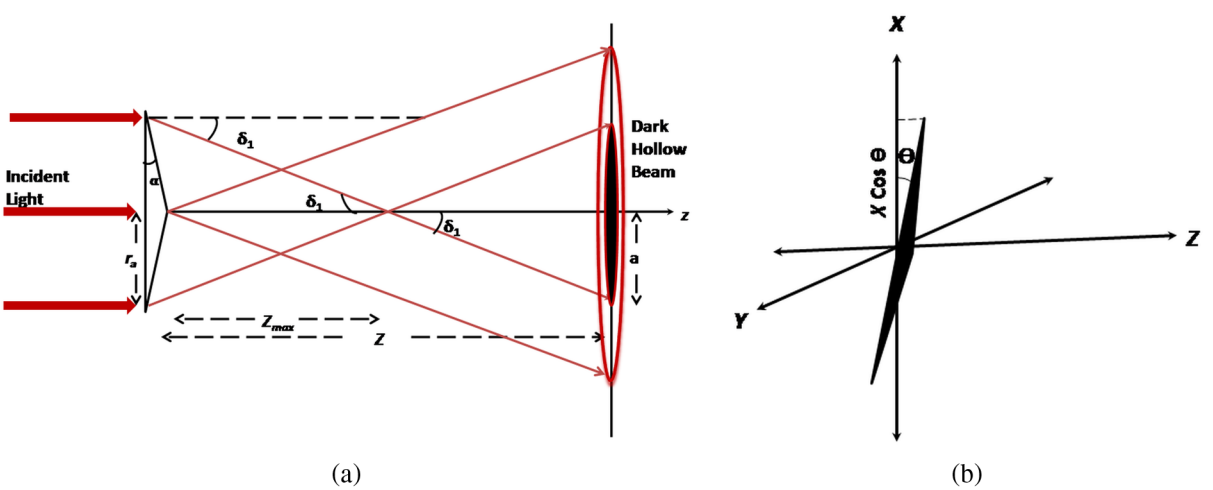


**Fig. 9** (a) Ray diagram of the formation of DHB at a distance $Z$ from axicon. In the diagram $\alpha$ and $r_a$ are the alpha angle and radius of the axicon, respectively, $\delta_1$ is the angle of deviation and $Z_{\max}$ is the focal depth of axicon. The width of the dark region of DHB is "$a$." (b) Tilted axicon makes an angle of $\Theta$ with the $x$-axis.

assembly in the direction of incident rays is defined as $\delta = \delta_1 + \delta_2$. Where $\delta_2 = \text{ArcTan}\ (h/f)$ is the deviation due to the thin converging lens of focal length $f$. Here, $h$ is the incident point for light rays in the lens plane. In axicon-lens assembly, $h$ is defined as $h = r_a - Z_0 \text{Tan}\,\delta_1$, where $Z_0$ is the distance between axicon and lens. Now the width of the dark region in DHB for $x$- and $y$-axes are expressed as

$$a_x = (x\,\text{Cos}\,\Theta - Z_0\,\text{Tan}[(n-1)\alpha])\left(\frac{Z}{Z_{\max X}} - 1\right), \tag{10}$$

$$a_y = (y - Z_0\,\text{Tan}[(n-1)\alpha])\left(\frac{Z}{Z_{\max Y}} - 1\right), \tag{11}$$

where $Z_{\max X} = \frac{x\,\text{Cos}\,\Theta - Z_0\,\text{Tan}[(n-1)\alpha]}{\text{Tan}\,\delta}$ and $Z_{\max Y} = \frac{y - Z_0\,\text{Tan}[(n-1)\alpha]}{\text{Tan}\,\delta}$ are the focal depths in two directions after axicon-lens assembly, respectively.

Now, on substituting the values of $a_x$ and $a_y$ in Eq. (9), we can calculate the eccentricity of the dark region of DHB for axicon-lens assembly.

$$e = \left[1 - \left(\frac{\{x\,\text{Cos}\,\Theta - Z_0\,\text{Tan}[(n-1)\alpha]\}\left\{\frac{Z}{\frac{x\,\text{Cos}\,\Theta - Z_0\,\text{Tan}[(n-1)\alpha]}{\text{Tan}\,\delta}} - 1\right\}}{\{y - Z_0\,\text{Tan}[(n-1)\alpha]\}\left\{\frac{Z}{\frac{y - Z_0\,\text{Tan}[(n-1)\alpha]}{\text{Tan}\,\delta}} - 1\right\}}\right)^2\right]^{1/2}. \tag{12}$$

Equation (13) shows the theoretical formula for calculating the variation in the elliptical shape of the dark cavity of the beam generated from the axicon-lens assembly.

The simulation shows that the variation in the eccentricity of the dark region is a function of $\Theta$ and $Z$. For a fixed point in the propagation distance $Z$ ($Z > Z_{\max}$), the eccentricity increases with an increase in the $|\Theta|$; however, the value of eccentricity of the dark region decreases with $Z$ at fixed $\Theta$ [as calculated using Eq. (9) and plotted in Fig. 10(a)].

From Eq. (12), similar variations in the elliptical shape of the dark cavity of EDHB with change in $Z$ and $\Theta$ can be observed for both cases (axicon and axicon-lens assembly), whereas in the later case the eccentricity of the beam reduces [as represents in Figs. 10(a) and 11(a)]. As one can predict, the expansion of the EDHB with propagation distance is enhanced on introducing converging lens in front of axicon (i.e., axicon-lens assembly), see Figs. 10(b) and 11(b).

The eccentricity of the dark region of DHB was calculated at different values of $\Theta$, keeping $Z$ and $Z_0$ fixed. Figure 12 shows variation in eccentricity of dark cavity of EDHB at different values of $\Theta$. Although tilting axicon, one should care to keep the position of the lens intact to attain perfect control over the shape of dark cavity of the EDHB.

The experimental and theoretical outcomes show similar phenomena of increasing eccentricity of DHB as a function of $\Theta$ and results in the generation of EDHB using axicon-lens assembly as shown in Fig. 12(B). The variation in the experimental and theoretical data may be attributed to the experimental conditions and thin lens approximation in theoretical calculations.

*Tilted axicon-lens doublet*. The Fresnel diffraction integral in Eq. (2) can be solved for on-axis illuminated axicon-lens doublet and expressed as[24]

$$U(r', z) = \frac{k}{z}\int_0^{R_a} U_1(r, 0)\exp\left\{-\frac{ikr^2}{2z}\right\} J_0\left(\frac{kr'r}{z}\right) r dr. \tag{13}$$

In the Eq. (13), $R_a$ is the axicon aperture, whereas $r' = (x'^2 + y'^2)^{1/2}$ and $r = (x^2 + y^2)^{1/2}$ are representing

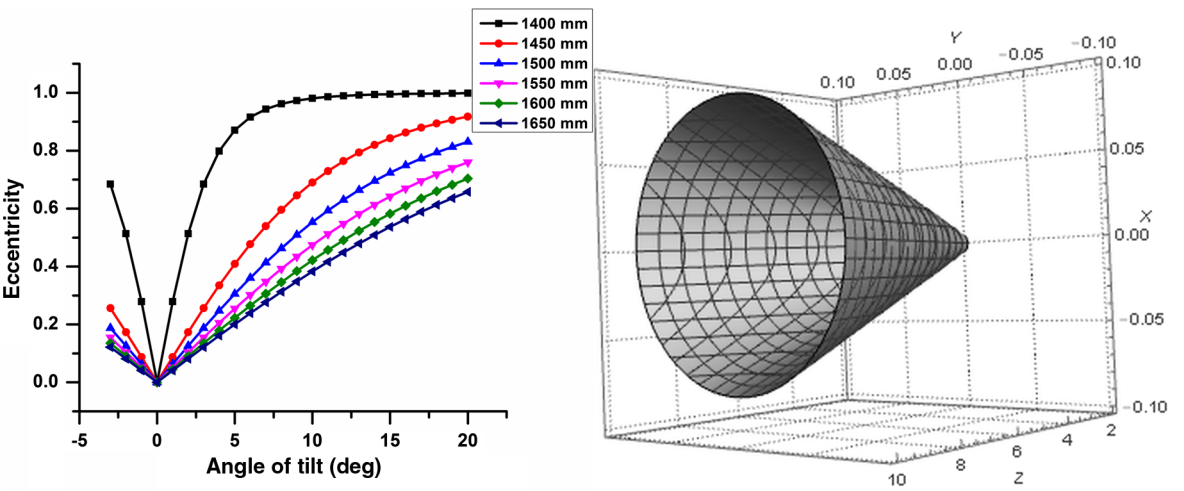


**Fig. 10** Variation in the (a) eccentricity of the dark region of EDHB with change in $Z$ and $\Theta$, respectively, and (b) shape of the EDHB with propagation distance $Z$, keeping $\Theta = 20$ deg constant in the case of axicon.

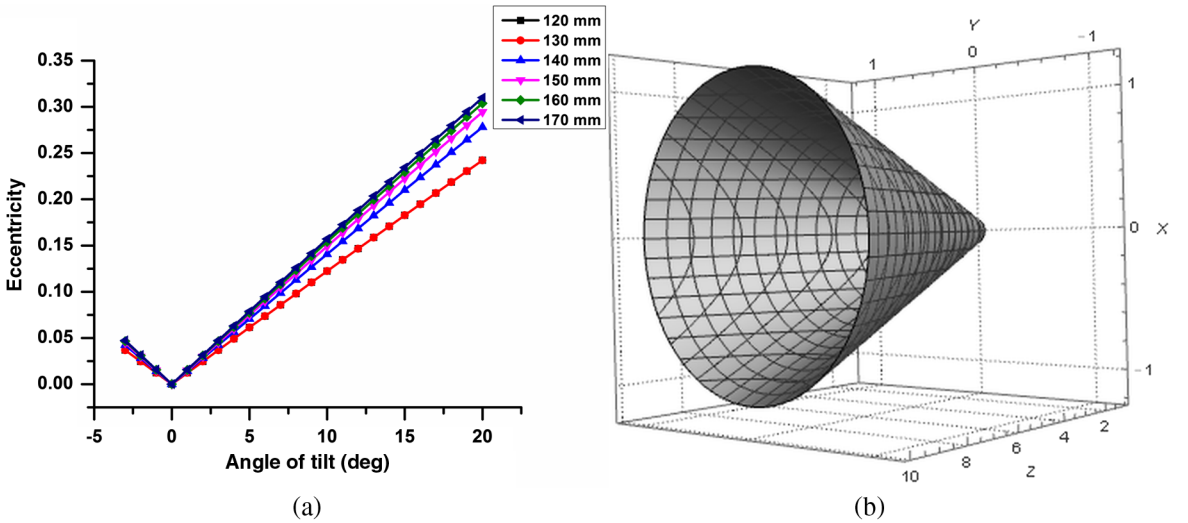


**Fig. 11** Numerical simulation of (a) the variation in the eccentricity of the dark region of EDHB with change in $Z$ and $\Theta$, respectively, and (b) variation in the shape of EDHB with $Z$, keeping $\Theta = 20$ deg constant in axicon-lens assembly. The values for $Z_0$ and $f$ were fixed at 100 and 120 mm, respectively.

positions on observation and axicon-lens doublet plane, respectively. $U_1\ (r,0)$ is the product of the light field illuminated at the incident plane, $U_0\ (r,0)$ and transmission function of axicon-lens doublet, $U_{Ax}(r,0) = \exp\{-ik[(-r^2/2f + (n-1)\alpha r]\}$.

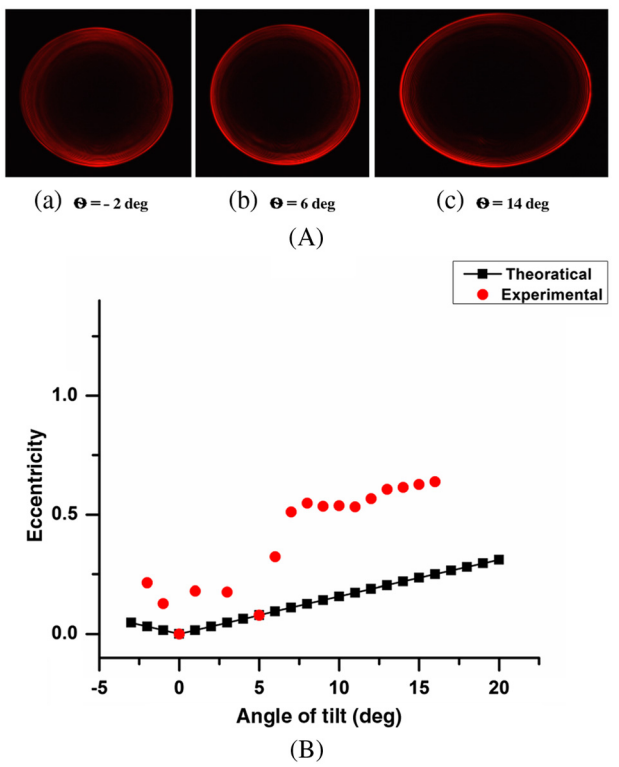


**Fig. 12** (A) (a)–(c) CCD images effect of the $\Theta$, on the shape of dark region in the EDHB keeping the position of the lens intact, (B) variation in eccentricity of the dark region of DHB with $\Theta$ at $Z = 170$ mm. Red circular dots and black square dots in solid line represent experimental and theoretical results, respectively.

Thus, $U_1\ (r,0)$ can defined as

$$U_1(r,0) = U_0(r,0)\exp\left\{-ik\left[-\frac{r^2}{2f} + (n-1)\alpha r\right]\right\}. \quad (14)$$

In the case of oblique illuminated Gaussian beam, $U_0\ (r,0)$ can expressed in terms of Cartesian coordinate $(x,y)$ as

$$U_0(x,y,0) = I_0^{1/2}\exp\left\{-\frac{ik(x^2\,\mathrm{Cos}^2\,\Theta + y^2)}{2q}\right\}, \quad (15)$$

where $1/q = 1/R - 2i/kW^2$, $W = W_0[1 + (d/Z_r)^2]^{1/2}$ is the beam waist, $R = d[1 + (Z_r/d)^2]$ is the radius of wavefront curvature, $I_0 = 2E/(\pi W^2)$ is the intensity of the on-axis beam, and $E$ is the total energy, respectively. Here, $d$ is the propagation distance between laser and axicon-lens doublet, $Z_r = \pi W_0^2/\lambda$, and $W_0$ is the minimum beam waist.

To obtain the solution of oblique illuminated axicon-doublet, Eqs. (14) and (15) are substituted in Eq. (13). To further simplify the integral, it requires some complex calculations, which make it tedious work. Therefore, to simplify the complicacy, we substituted $y = 0$ and calculated the effect of obliquely illuminated axicon on the radial intensity distribution of the focused hollow ring of radius $R_0$. In the case of axicon-lens doublet, the ring radius at $Z = f$ is calculated by substituting $Z_0 = 0$ mm in Eq. (11); therefore, the ring radius comes out to be $R_0 = f\,\mathrm{Tan}\,\delta - x\,\mathrm{Cos}\,\Theta$. At $f \gg x$, the ring radius reduces to $R_0 = f(n-1)\alpha - x\,\mathrm{Cos}\,\Theta$. The second term $x\,\mathrm{Cos}\,\Theta$ can be neglected for constant $\Theta$; however, in the case of varying oblique illumination it plays a major role.

The radial intensity distribution of EDHB generated at the focus of the doublet is defined as

$$I(x',f) = |U(x',f)|^2, \quad (16)$$

$$I(x',f)=\frac{0.24EW_x}{R_0\lambda f}\frac{\left|F\left(\frac{\rho}{(1+i\Delta)^{1/2}}\right)\right|^2}{(1+\Delta)^{3/4}}, \tag{17}$$

where $\rho=(R_0\pi W_x/2\lambda f)[1-(x'/R_0)^2]$, $\Delta=\pi W_x/\lambda R_x$, $W_x=W_0\,\mathrm{Cos}\,\Theta[1-(d/Zr)^2]^{1/2}$, and $R_x=d\,\mathrm{Cos}^2\,\Theta[1-(Zr/d)^2]^{1/2}$. Also, $F(c)$ is the sum of two confluent hypergeometric functions; $F(c)=1F1\left(\begin{matrix}\frac{3}{4}\\ \frac{1}{2}\end{matrix}|\,-c^2\right)-\frac{i\Gamma(\frac{5}{4})}{\Gamma(\frac{3}{4})}\,c\;1F1\left(\begin{matrix}\frac{5}{4}\\ \frac{3}{2}\end{matrix}|-c^2\right)$.

To compare the parameters (such as width, radius, and intensity) of EDHB ($\Theta\neq 0$) with on-axis DHB, its radial intensity distributions are normalized with respect to circular-DHB ($\Theta=0$). Also, the values of $n$, $\alpha$, and $W_0$ are 1.515, 0.0174, and 0.74 mm, respectively (Fig. 13).

As shown in Figs. 14 and 15, numerical results have shown that the effect of oblique illumination on the parameters of high-intensity ring generated at the focus of axicon-lens doublet is minor at small values of $\Theta$; however, it increases rapidly at large values of $\Theta$.

The high-intensity ring formed at the focal plane of axicon-lens doublet has already shown its potential applications in the field of corneal surgery[23] and atoms trapping.[50] Therefore, fine control over the ring parameters may enhance the compatibility of the beam. Also, the ring width of the DHB generated from an ideal axicon remains constant for large propagating distance in free space (ring width–radius of the beam falling on the incident plane of axicon).[52] Similar features are also observed geometrically in astigmatic hollow beam (EDHB), generated from tilted axicon (in both on-axis and tilted axicon, angle of deviation introduced by axicon lens is constant for all rays passing through upper and lower part of axicon, respectively); hence, its detailed investigation could enhance its importance in the field of free-space communication, as the astigmatic hollow beams are shown to be less influenced to the atmospheric turbulence.[26]

### 3.3 *Short-Range Nondiverging Optical Array Optical Generator*

The comprehensive study of the geometrical constraints of obliquely illuminated axicon performed and utilized to propose an SRNOA optical generator; also capable of delivering long-range optical array, Bessel–Gaussian beam of desired length and controlled elliptical/circular symmetric hollow beams. The proposed design is similar to the experimental setup explained in Sec. 2 with few modifications such as axicon and converging lens are placed on computer operating 2-D mounts that allow precise movements to the respective optical elements. The stage "$S1$" $(x,\Theta)$ controls the position of axicon to generate SRNOA and circular/elliptical DHB with desired dimensions and eccentricity, respectively. Although stage "$S2$" $(x,z)$ enable precise variations in the position of the converging lens in axicon-lens assembly to change the dimension of the optical array generated after bottle cavity (see Sec. 3.1), length of bottle cavity, and Gaussian–Bessel beam in a controlled manner.[16] The output beam is passed through computer-operated VNDF to control the intensity falling on the CCD. The generator is designed

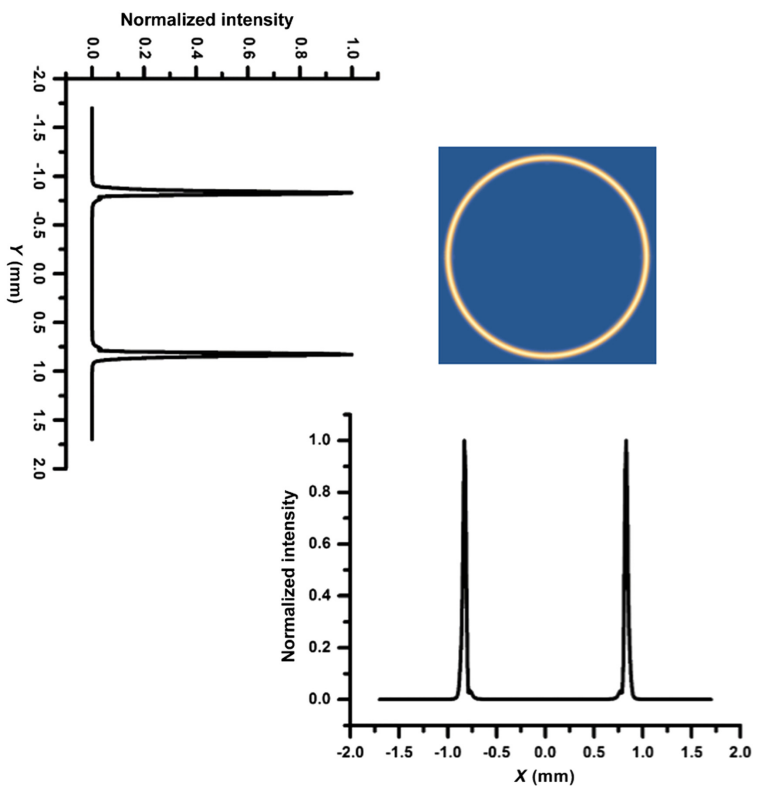


**Fig. 13** Calculated on-axis high-intensity DHB at focus of axicon-lens doublet ($\Theta=0$ deg) using Eq. (17).

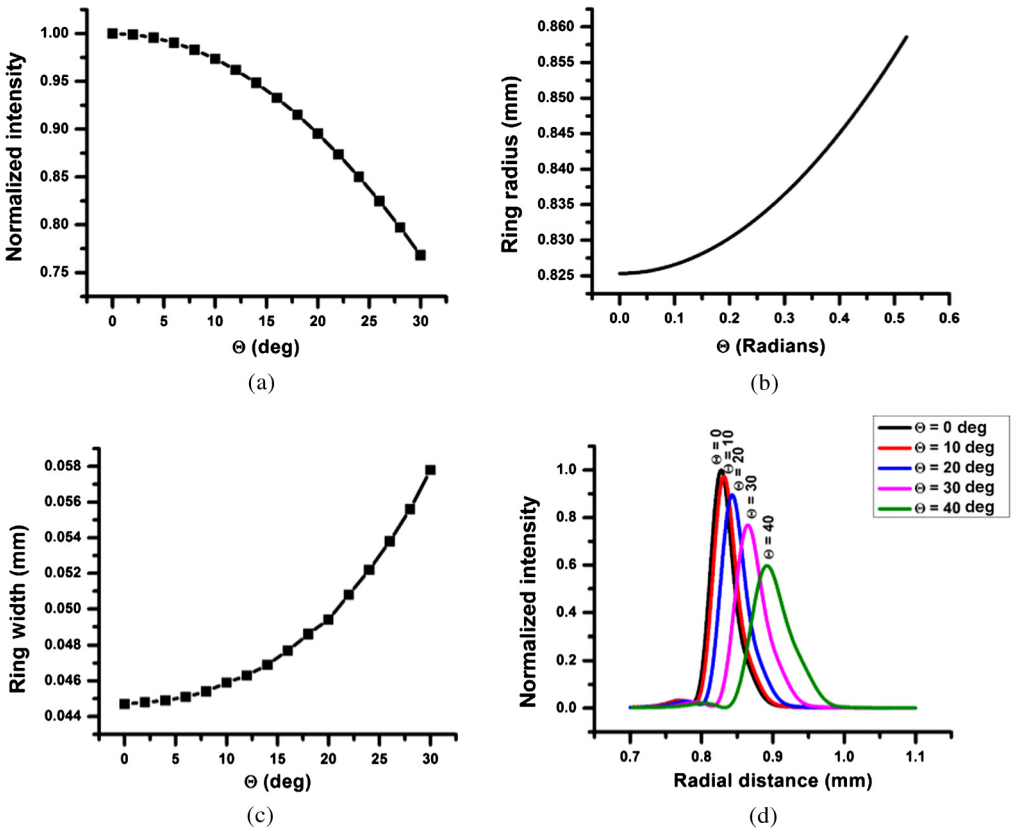


**Fig. 14** Theoretical results showing effect of change in Θ on ring parameters; (a) normalized intensity at $R_0$, (b) radius, (c) width, and (d) radial intensity distribution centered at $R_0$ of the ring.

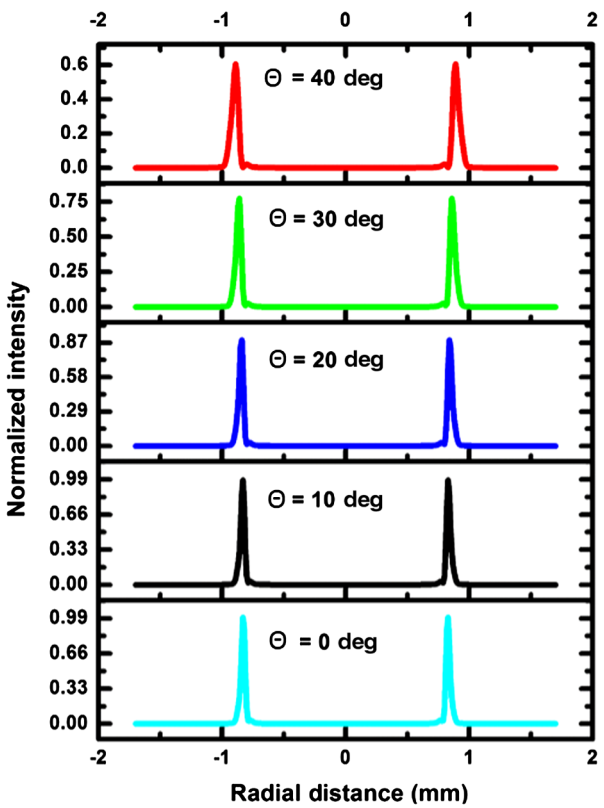


**Fig. 15** Normalized radial intensity distribution of EDHB at the focus of axicon-lens doublet at different values of Θ.

for monochromatic laser source; however, polychromatic light field can also be used with few changes in design such as introducing pinhole between source and axicon to build spatial coherence.

## 4 Conclusion

In the present study, a convenient method for generating nondiverging optical array for a short range of propagation distance is discussed. The aberration spots and elliptical hollow beam have been studied experimentally using axicon in oblique illumination geometry, wherein these bright spots appeared in a symmetric pattern of transverse optical array in the focal depth. However, the aforementioned pattern reappears beyond the hollow cavity of bottle beam with a fixed number of aberration spots. The width of the focal spots remains invariant for a short range of propagation distance within the focal depth of axicon system and has shown resemblance to the well-known pattern of optical modes generated from complex setups. As the dimensions of the optical array in the focal depth region and the shape of the dark region in elliptical hollow beam are varying as a function of propagation distance and angle of tilt of axicon, therefore, can be controlled by the combination of these two parameters. In addition, theoretical simulations are also performed to analyze the propagation dynamics of SRNOA and the generation of noncircular hollow beam due to oblique illumination of axicon, which is in agreement with experimental results. The results are summarized in the form of a short-range nondiverging optical array generator, also capable of producing Bessel beam, elliptical/circular symmetric

hollow beams, and long-range optical array with a fixed number of bright spots. The high-intensity-focused ring generated from axicon-lens doublet has shown its significance in corneal eye surgery and laser machining; hence, the generation/removal of EDHB with controlled parameters (intensity, ring width, and radius) could enhance its application. Although the optical arrays may show promising applications in free-space optical communication, optical imaging, and data processing when accompanied with extensive theoretical analysis, and would be included in future reports.

## Acknowledgments

The authors thank the Director and Divisional Review Committee (DRC), CSIR-National Physical Laboratory, New Delhi, for granting the permission to publish this work.

## References

1. H. Nagar et al., "Non-diffracting beams for label-free imaging through turbid media," *Opt. Lett.* **43**(2), 190–193 (2018).
2. T. A. Planchon et al., "Rapid three-dimensional isotropic imaging of living cells using Bessel beam plane illumination," *Nat. Methods* **8**(5), 417–423 (2011).
3. R. E. Meyers et al., "Virtual ghost imaging through turbulence and obscurants using Bessel beam illumination," *Appl. Phys. Lett.* **100**(6), 061126 (2012).
4. N. Weber et al., "Highly compact imaging using Bessel beams generated by ultraminiaturized multi-micro-axicon systems," *J. Opt. Soc. Am. A* **29**(5), 808–816 (2012).
5. A. Ashkin et al., "Observation of a single-beam gradient force optical trap for dielectric particles," *Opt. Lett.* **11**(5), 288–290 (1986).
6. V. Garcés-Chávez et al., "Transfer of orbital angular momentum to an optically trapped low-index particle," *Phys. Rev. A* **66**(6), 063402 (2002).
7. G. Zhang et al., "Femtosecond laser Bessel beam welding of transparent to non-transparent materials with large focal-position tolerant zone," *Opt. Express* **26**(2), 917–926 (2018).
8. X. Zhang, B. Zhao, and Z. Li, "Measurement method of spatial straightness error using non-diffracting beam and moiré-fringe technology," *J. Opt. A: Pure Appl. Opt.* **6**(1), 121–126 (2003).
9. K.-S. Lee and J. P. Rolland, "Bessel beam spectral-domain high-resolution optical coherence tomography with micro-optic axicon providing extended focusing range," *Opt. Lett.* **33**(15), 1696–1698 (2008).
10. D. G. Grier, "A revolution in optical manipulation," *Nature* **424**(6950), 810–816 (2003).
11. V. Belyi et al., "Bessel-like beams with z-dependent cone angles," *Opt. Express* **18**(3), 1966–1973 (2010).
12. D. McGloin and K. Dholakia, "Bessel beams: diffraction in a new light," *Contemp. Phys.* **46**(1), 15–28 (2005).
13. P. Saari and K. Reivelt, "Evidence of X-shaped propagation-invariant localized light waves," *Phys. Rev. Lett.* **79**(21), 4135–4138 (1997).
14. M. Mazilu et al., "Light beats the spread: "non-diffracting" beams," *Laser Photonics Rev.* **4**(4), 529–547 (2010).
15. Y. Wang et al., "Electromagnetic diffraction theory of refractive axicon lenses," *J. Opt. Soc. Am. A* **34**(7), 1201–1211 (2017).
16. M.-D. Wei, W.-L. Shiao, and Y.-T. Lin, "Adjustable generation of bottle and hollow beams using an axicon," *Opt. Commun.* **248**(1), 7–14 (2005).
17. H. S. Lee et al., "Holographic nondiverging hollow beam," *Phys. Rev. A* **49**(6), 4922–4927 (1994).
18. C. Paterson and R. Smith, "Higher-order Bessel waves produced by axicon-type computer-generated holograms," *Opt. Commun.* **124**(1–2), 121–130 (1996).
19. N. Chattrapiban et al., "Generation of nondiffracting Bessel beams by use of a spatial light modulator," *Opt. Lett.* **28**(22), 2183–2185 (2003).
20. J. Yin et al., "Optical potential for atom guidance in a dark hollow laser beam," *J. Opt. Soc. Am. B* **15**(1), 25–33 (1998).
21. Z. Luo et al., "Femtosecond laser highly-efficient plane processing based on an axicon-generated donut-shaped beam," *Chin. Opt. Lett.* **16**(3), 031401 (2018).
22. P. Xu et al., "Trapping a single atom in a blue detuned optical bottle beam trap," *Opt. Lett.* **35**(13), 2164–2166 (2010).
23. J. Arlt and M. J. Padgett, "Generation of a beam with a dark focus surrounded by regions of higher intensity: the optical bottle beam," *Opt. Lett.* **25**(4), 191–193 (2000).
24. O. Ren and R. Birngruber, "Axicon: a new laser beam delivery system for corneal surgery," *IEEE J. Quantum Electron.* **26**(12), 2305–2308 (1990).
25. P.-A. Bélanger and M. Rioux, "Ring pattern of a lens-axicon doublet illuminated by a Gaussian beam," *Appl. Opt.* **17**(7), 1080–1088 (1978).
26. Y. Chen et al., "Scintillation properties of dark hollow beams in a weak turbulent atmosphere," *Appl. Phys. B* **90**(1), 87–92 (2008).
27. B. Vohnsen, S. Castillo, and D. Rativa, "Wavefront sensing with an axicon," *Opt. Lett.* **36**(6), 846–848 (2011).
28. R. Arimoto et al., "Imaging properties of axicon in a scanning optical system," *Appl. Opt.* **31**(31), 6653–6657 (1992).
29. A. Thaning, Z. Jaroszewicz, and A. T. Friberg, "Diffractive axicons in oblique illumination: analysis and experiments and comparison with elliptical axicons," *Appl. Opt.* **42**(1), 9–17 (2003).
30. C. Geng et al., "Coherent beam combination of an optical array using adaptive fiber optics collimators," *Opt. Commun.* **284**(24), 5531–5536 (2011).
31. L. Zeng et al., "High data rate multiple input multiple output (MIMO) optical wireless communications using white LED lighting," *IEEE J. Sel. Areas Commun.* **27**(9), 1654–1662 (2009).
32. V. Jolivet et al., "Beam shaping of single-mode and multimode fiber amplifier arrays for propagation through atmospheric turbulence," *IEEE J. Sel. Top. Quantum Electron.* **15**(2), 257–268 (2009).
33. T. J. Cloonan, "Architectural considerations for optical computing and photonic switching," in *Optical Computing Hardware: Optical Computing*, J. Jahns and S. H. Lee, Eds., pp. 1–14, AT&T-Academic Press Inc. (2014).
34. J.-H. Hsu, C.-H. Lee, and R. Chen, "A high-efficiency multi-beam splitter for optical pickups using ultra-precision manufacturing," *Microelectron. Eng.* **113**, 74–79 (2014).
35. J. E. Curtis, B. A. Koss, and D. G. Grier, "Dynamic holographic optical tweezers," *Opt. Commun.* **207**(1), 169–175 (2002).
36. J. Liesener et al., "Multi-functional optical tweezers using computer-generated holograms," *Opt. Commun.* **185**(1), 77–82 (2000).
37. P. C. Mogensen and J. Glückstad, "Dynamic array generation and pattern formation for optical tweezers," *Opt. Commun.* **175**(1), 75–81 (2000).
38. J. Zhang, C. Zhou, and X. Wang, "Three-dimensional profilometry using a Dammann grating," *Appl. Opt.* **48**(19), 3709–3715 (2009).
39. M. Downs and J. Jahns, "Integrated-optical array generator," *Opt. Lett.* **15**(14), 769–770 (1990).
40. A. Sabatyan and J. Rafighdoost, "Grating-and checkerboard-based zone plates as an optical array generator with a favorable beam shape," *Appl. Opt.* **56**(19), 5355–5359 (2017).
41. S. Vyas and P. Senthilkumaran, "Interferometric optical vortex array generator," *Appl. Opt.* **46**(15), 2893–2898 (2007).
42. U. G. R. Grunwald et al., "Generation of femtosecond Bessel beams with microaxicon arrays," *Opt. Lett.* **25**(13), 981–983 (2000).
43. R. Stevenson et al., "Binary-phase zone plate arrays for the generation of uniform focal profiles," *Opt. Lett.* **19**(6), 363–365 (1994).
44. T. Tanaka and S. Yamamoto, "Comparison of aberration between axicon and lens," *Opt. Commun.* **184**(1), 113–118 (2000).
45. M. Born and E. Wolf, *Principles of Optics*, 7th ed., Cambridge University Press, Cambridge, U.K. (1999).
46. Z. Jaroszewicz et al., "Programmable axicon for variable inclination of the focal segment," *J. Mod. Opt.* **51**(14), 2185–2190 (2004).
47. S. Berdagué and P. Facq, "Mode division multiplexing in optical fibers," *Appl. Opt.* **21**(11), 1950–1955 (1982).
48. J. Courtial and M. Padgett, "Performance of a cylindrical lens mode converter for producing Laguerre–Gaussian laser modes," *Opt. Commun.* **159**(1), 13–18 (1999).
49. E. Abramochkin and V. Volostnikov, "Generalized gaussian beams," *J. Opt. A: Pure Appl. Opt.* **6**(5), S157 (2004).
50. J. Arlt et al., "Optical dipole traps and atomic waveguides based on Bessel light beams," *Phys. Rev. A* **63**(6), 063602 (2001).
51. Z. Mei and D. Zhao, "Decentered controllable elliptical dark-hollow beams," *Opt. Commun.* **259**(2), 415–423 (2006).
52. C. Bangwei et al., "Propagation and transformation properties of axicon optical systems for laser beams," *Chin. J. Lasers* **21**(1), 21–25 (1994).

**Rajeev Dwivedi** received his MSc in physics from Jamia Millia Islamia, New Delhi, in 2014 and began his research work in 2015. He is a PhD research student under the supervision of Dr. Parag Sharma in CSIR-National Physical Laboratory New Delhi, India. He has interest in lasers, singular optics, and polarization optics.

**Parag Sharma** received his MSc and PhD degrees in physics from Dayalbagh Educational Institute, India, in 2002 and 2006, respectively. He is working as a scientist in CSIR-National Physical Laboratory, India, since 2007. He was awarded NN Saha Award by the Indian Biophysical Society, in 2003, ISCA-Young Scientist Award, and "DST-Award" for participation in 18th Meeting of Nobel Laureates and Students, Germany, in 2004, and Dr. O.P.S. Sengar Memorial Young Scientist Award in 2015.

**Virendra Kumar Jaiswal** received his MSc and MTech degrees in physics and applied optics from Allahabad University and IIT Delhi, India, in 2000 and 2002, respectively. He has worked in area of lasers and quantum optics as scientist with Physical Research Laboratory, Ahmedabad and has mainly contributed in the area of singular optics and polarization optics. Currently, he is working with CSIR-National Physical Laboratory, India, as senior scientist and his research interests include applied and laser photonics.

**Ranjana Mehrotra** received her PhD in biophysics from IIT Delhi, India, in 1986. She is chief-scientist and head, Physico-Mechanical Metrology Division in CSIR-National Physical Laboratory, India. Her research interest includes bio-photonics, vibrational spectroscopy, and nanoscopy.